Supercontinuum comb generated by soliton molecule pulse laser injecting into a nonlinear amplifying loop mirror

Renlai Zhou,[a,b,*] Shijie Chen,[b] Qian Li,[b,**] H. Y. FU,[c] K. Nakkeeran,[d]

[a]*Key Laboratory of In-Fiber Integrated Optics, Ministry Education of China, Harbin Engineering University, Harbin 150001, China*
[b]*School of Electronic and Computer Engineering, Peking University, Shenzhen 518055, China*
[c]*Tsinghua Shenzhen International Graduate School and Tsinghua-Berkeley Shenzhen Institute, Tsinghua University, Shenzhen 518055, China*
[d]*School of Engineering, Fraser Noble Building, University of Aberdeen, Aberdeen AB24 3UE, UK*
[*]*zrlhit@126.com*
[**]*liqian@pkusz.edu.cn*

Abstract: Very first time, we experimentally demonstrated the generation of supercontinuum (SC) comb by pumping a tunable soliton molecule fiber laser output signal into a nonlinear amplifying loop mirror (NALM). SC signals with different comb-teeth structures were obtained by controlling the pump power and waveplate orientation of the polarization-maintained soliton molecule fiber laser. The maximum achieved output powers of dual SC combs from two ports were 21.95 (output 1) and 3.75 mW (output 2), respectively. The spectral and temporal profiles of the SC comb were compared with the simulation results and the first-order coherence was evaluated. Our experiment provides a novel technique for the generation of SC signal with various comb-teeth structures that can be utilized in broadband spectrometers and full-field 3D metrology.

Key Words: Supercontinuum comb; soliton molecule; mode-locked fiber laser; nonlinear optics

1. Introduction

Optical frequency combs (OFCs) with ultra-broadband, coherent, and equal frequency spanning spectrum have made conspicuous breakthrough in various fields, such as metrology [1], optical communications [2], and arbitrary optical waveform generation [3]. Broadband OFCs are normally generated through micro-resonator and highly nonlinearity fiber (HNLF). With the developments in the electron-beam lithography technique, the OFCs generated from micro-resonators outstand all other methods [4, 5]. However, it is necessary to address other challenges like low output power, device fabrication, stability, system integration and packaging [4]. On the other hand, broadband OFCs generation using HNLF can overcome these issues. Various methods were proposed to generate the supercontinuum (SC) comb using HNLF, such as discrete laser synthesizer [6, 7], mode-locked fiber laser [8, 9], and multistage electro-optic (EO) modulation scheme [10, 11] et al. To effectively generate SC comb by the laser synthesizer, the phase correlation among discrete lasers should be established, which increases the system complexity and its performance becomes very sensitive to various factors. Whereas, the EO modulator scheme was inherently a multistage setup, hence the experiment configuration was complicated and not cost effective.

Soliton molecules (SMs) is a fascinating nonlinear phenomenon observed in the mode-locking laser that is the coupled soliton pulses (SP) with a certain phase differences under comprehensive interactions. SMs were theoretically studied by the models of the coupled Ginzburg-Landau equation and nonlinear Schrödinger equation in fiber lasers [12]. The numerical investigation demonstrates the SM formation can refer to the direct soliton-soliton interaction as the oscillating tails overlapped, and the SMs can stably exist in the cavity when phase differences are 0, π, and $\pm\pi/2$. Heretofore, various SMs have been exemplified in mode-locked fiber lasers based on nonlinear polarization rotation (NPR) [13], nonlinear optical loop mirror (NOLM / NALM) [14, 15], real saturable absorbers (SAs) (e.g., graphene [16], carbon nanotubes [17, 18], MoS_2 / fluorine mica Langmuir Blodgett film [19]), nonlinear multimode interference effect [20], and spatiotemporal mode-locking [21] et al. In Ref. [22], the generation and propagation of various SMs were summarized, and pointed out that the SMs can be formed with fundamental unit of conventional solitons, stretched pulses, parabolic pulses, or gain-guided solitons. Universal mechanism for SM formation has been demonstrated in a ring fiber laser, and three different perturbations of third-order dispersion (dispersive wave generation), the periodic nature of the cavity (Kelly sidebands), and the random birefringence of the resonator were experimentally evidenced during the bound state formation [23]. Generally, the aforementioned soliton interactions coexist in the cavity, therefore numerous interesting SMs can be formed by complex soliton-soliton interactions in fiber lasers, namely soliton pairs, soliton triplets, soliton quartets, and multi-pulse bound soliton [24, 25]. For mode-locked fiber lasers, aforementioned various SMs with different phase differences could be generated using appropriate pump power and PC orientation in the cavity [13-25], but the complex soliton-soliton interactions in SMs formation are difficult to control and regulate.

Typical signature characteristic of the SM spectrum is the appearance of interference fringes with almost 100% modulation depth created by the coupling of coherent SP. This feature of SM mode-locked laser is similar to the discrete laser synthesizer with phase correlation that is utilized to generate SC combs. With this there emerges an open question of whether the SM mode-locked laser output signal can be injected into a segment of HNLF to generate SC combs?

In this work, pumping the output signal from a tunable SM fiber laser into a nonlinear amplifying loop mirror (NALM), we experimentally demonstrated the generation of broadband SC comb. The modulated spectra of SM in our proposed fiber laser can be tuned by controlling the pump power and waveplate orientation in the cavity, and the SC signals with different comb-teeth structures were generated and investigated. Numerical simulations were carried out to elucidate the dual SC combs formation in the NALM, and to evaluate the degree of first-order coherence of the generated SC comb.

2. Experiment setup

The experimental setup of the proposed SC comb generation was shown in Fig. 1. To generate the SM, a robust all polarization-

maintaining (PM) mode-locked fiber laser with a non-reciprocal phase bias was configured, as the setup enclosed within the dashed line in Fig. 1. A 976 nm laser diode (LD1) signal was launched into a high-gain 0.8 m PM-EDF (PM-ESF-7/125, Nufern) through a PM fiber 980/1550 nm wavelength-division multiplexer (WDM). The absorption coefficient of gain fiber was ~24 dB/m @ 976 nm. In order to improve the stability and coupling efficiency, two fiber collimators and a polarizing beam splitter (PBS) were integrated in the cavity. A λ/6 waveplate and a Faraday rotator (FR) were cascaded together to provide a non-reciprocal phase bias of 2π/3 to the signal for every roundtrip, and this maintained the fiber laser to operate at positive feedback reflection region, as a result, the self-starting ability of mode-locking was enhanced. The output mode-locking laser was injected into a NALM cavity through a fiber circulator. For the NALM gain amplification, a 1-m EDF (EDFL-980-HP, Nufern) was pumped by a 976 nm LD2 through a 980/1550 nm WDM. In order to generate the SC, a 585-m-long highly nonlinear fiber (HNLF) (NL-1550-Zero, YOFC) was inserted in the NALM. The output spectra and pulses train were measured by an optical spectrum analyzer (AQ6370D, Yokogawa) with a resolution of 0.02 nm, and a real-time oscilloscope (DSO-X 6004A, 20 GS/s, Keysight) with the help of a 3 GHz bandwidth InGaAs photodiode detector (PD). The radio frequency (RF) of laser operation was monitored by a signal analyzer (N9030B, Agilent) with a bandwidth from 3 Hz to 50 GHz. The average output power was measured by a power meter (S148C, Thorlabs) with 1 μW–1 W power range.

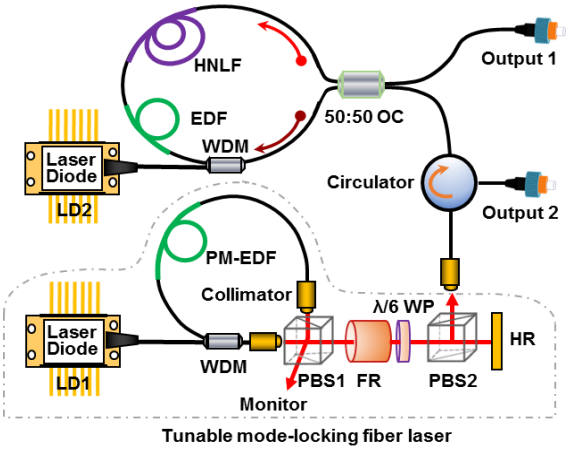

Fig. 1. Schematic diagram of dual SC combs generation in a NALM. All PM mode-locked fiber laser setup enclosed within dashed curve.

3. Experiment results

Through the strong birefringence in the cavity, a stable SM was self-started by fine adjustment of the orientation of λ/6 waveplate at a LD1 pump power of 400 mW. The output spectrum with periodic modulation was exhibited in Fig. 2(a), which was a typical feature of SP bound state interference with phase locking. The zoomed-in modulated spectrum was shown in Fig. 2(a), where the modulated period was $\Delta\nu = \Delta\lambda c/\lambda_0^2$ = 18.762 GHz, for $\Delta\lambda$ = 0.156 nm at λ_0 = 1579.876 nm, c is the speed of light in vacuum. A dip at spectral center indicates a ~ π phase difference between the adjacent SPs [17]. The corresponding intensity autocorrelation trace was depicted in Fig. 2(b), with $\Delta\tau$ = ~53.28 ps time separation between two close SPs, being consistent with the spectral modulated period ($\Delta\nu = 1/\Delta\tau$) in Fig. 2(a). Pulse duration of 1.63 ps was calculated with a sech^2 profile fit [see Fig. 2(b) inset]. The time separation between adjacent SP was more than five times of soliton duration, which made the direct soliton-soliton interaction very weak and the dynamics was dominated by the long-range interaction in the formation of bound-state pulses [26]. The oscilloscope trace of the pulse train was presented in Fig. 2(c), which has a ~11.55 ns interval period, which is consistent with the roundtrip time of the laser cavity. The screen-shot of pulse train with 5 μs time range was shown in the inset of Fig. 2(c), which evidenced the single pulse energy was steady. As depicted RF spectrum in Fig. 2(d), the pulse repetition rate was 86.47787 MHz with a 1 Hz resolution-bandwidth (RBW), and the SNR was over 78 dB, which confirmed the good stability of the SM operation. Up to 2 GHz wideband RF spectrum presented in the inset of Fig. 2(d), further revealed that the SM operated in a highly stable regime.

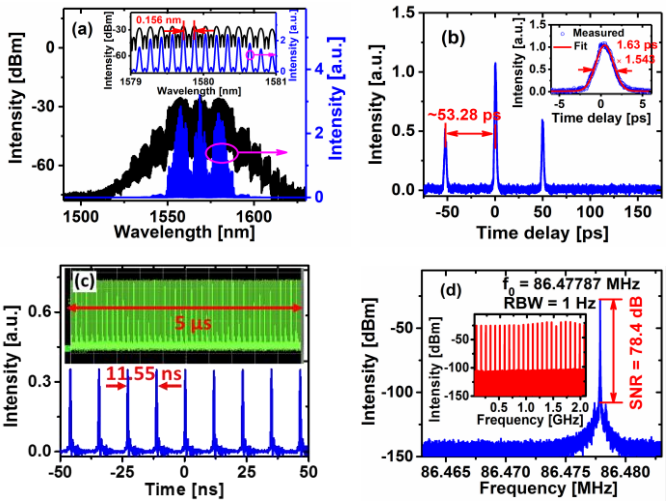

Fig. 2. Experiment results of a soliton pairs molecule: (a) optical spectra in log-scale as black curve, linear scale as blue curve; (b) intensity AC trace; (c) output pulses train; (d) RF spectra.

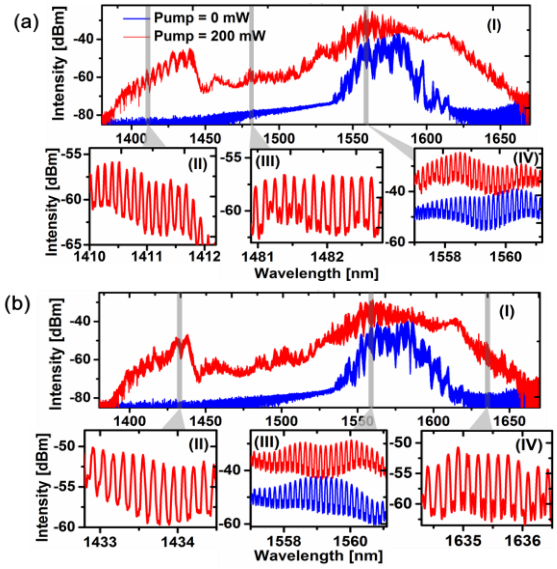

Fig. 3. Measured output spectra of the SC combs: (a) total spectrum (I) and enlarged spectra (II)-(IV) at output 1; (b) total spectrum (I) and enlarged spectra (II)-(IV) at output 2.

After injecting SM into the NALM, the monitored initial output powers were 0.422 and 0.304 mW at outputs 1 and 2, and the corresponding output spectra were depicted as blue curves in Figs. 3(a)(I) and 3(b)(I). Compared with the source SM spectrum, a modulated pattern was noted in the NALM output spectra due to the constructive interference between the two beams of counter propagating in the NALM. Increasing the LD2 power to 200 mW, SC combs were formed at outputs 1 and 2, and the measured output spectra were presented as red curves in Figs. 3(a)(I) and

3(b)(I). The overall spectral profiles of the dual SC combs were similar to each other in the wavelength range of 1385-1660 nm, but the intensity fluctuations were different. The enlarged spectra at 1410–1412.2 nm, 1480.9–1482.8 nm, and 1557–1561.2 nm were shown in Figs. 3(a)(II)–(IV) and 1432.8–1435.5 nm, 1557–1561.2 nm, and 1634.2–1636.5 nm were shown in Figs. 3(b)(II)–(IV). The frequency interval between adjacent comb teeth was fixed with ~18.76 GHz which was consistent with the spectral modulated period of the SM spectrum. Noted that the spectral profile of the generated SC combs was not flat, and this result can be explained by the following reasons. Firstly, the combined effect of dispersion (SM central wavelength located at the anomalous dispersion region of HNLF) and the nonlinear effects might have caused the spectral unevenness [27, 28]. Secondly, when the SM propagates in the HNLF, the amplification of random noise through modulation instability might be detrimental to the spectral flatness. Finally, the coherent interference of sidebands in the spectrum of pump SM signal in the arms of the NALM could have caused the spectral unevenness. Solitons separating from accompanying Kelly sidebands has been demonstrated in a mode-locked fiber laser [29], and we consider the spectral flatness may be improved by this technique.

To investigate the influence of LD2 pump power in the formation of SC combs, we measured the output spectra at output 1, 2 under different LD2 pump powers, and the results were shown in Figs. 4(a). It was evident that the SC combs spectra were gradually broadened with the increase of LD2 pump power due to the soliton self-frequency shift in red-side and the dispersive wave emission in the blue-side. Typical dispersive wave emission and the Raman spectrum were obvious at LD2 pump powers of 100 and 200 mW. Output spectra for the wavelength ranges 1387.9–1394.5 nm and 1669.9–1685 nm was shown in the first row in Fig. 4(a) corresponding to the LD2 pump power of 400 mW. In here, the comb-teeth fluctuations could still appear in the blue-side, and disappeared in the red-side. This contrast implied the deterioration of SC comb spectral coherence. The smoothing of the comb-teeth in the red-side maybe results from the cascade stimulated Raman scattering during the SC generation in HNLF [30]. From the obtained results, it is obvious that the bandwidth, flatness and comb-teeth depth of the SC comb need to be further improved, which can be optimized by managing the length and dispersion of HNLF in NALM. Average output powers were measured at both outputs for various LD2 pump powers and depicted in Fig. 4(b). It was found that the average output 1 power grew linearly with LD2 pump power, and the maximum achieved output power was 21.95 mW at LD2 pump power of 400 mW. On the other hand, the average output 2 power tends to saturate with increase of LD2 pump power with a maximum value reached as 3.75 mW.

Also from the experimental results, we found that the comb-teeth structure of the generated SC signal depends on the modulated spectrum of SM. Our group has experimentally demonstrated the various SMs in this robust all PM mode-locked fiber laser, the strong birefringence in the cavity is more favorable for the formation of SMs [24]. Through adjustments of the λ/6 waveplate and LD1 power, we observed

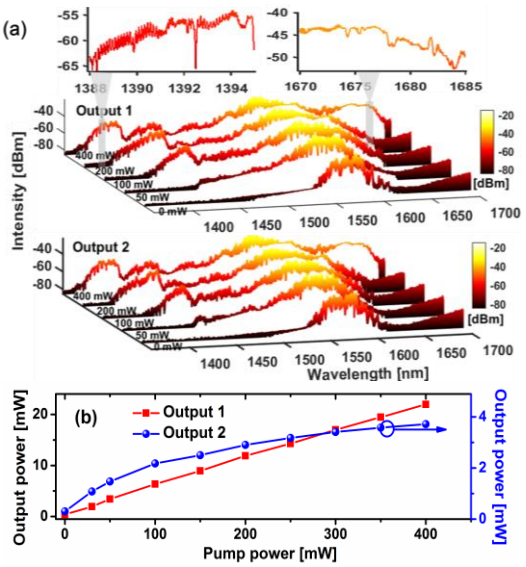

Fig. 4. (a) Measured output spectra of output 1, 2 at different pump powers; (b) monitored average output powers of output 1, 2 versus pump powers.

single SP and multi-pulse SM at different settings, and the monitored intensity autocorrelation traces were shown in Figs. 5(c) and 5(d), respectively. When the single SP was injected to the NALM, the measured output 1 and 2 powers were 0.385 and 0.265 mW, respectively. With LD2 pump power set to 200 mW, the measured output spectrum (red curve) was as shown in Fig. 5(a). Compared to the mode-locked laser SP spectrum (blue curve), the SC comb spectrum was quite broadened, but the comb-like structure was not observed, as shown in the inset of Fig. 5(a). Now, adjusting the λ/6 waveplate in the mode-locking fiber laser, the multi-pulse SM was generated and launched into the NALM, the comb-teeth structure [Fig. 5(b)] was formed at both outputs 1 and 2 with LD2 power level unaltered. Features of secondary modulation were observed in the output spectra [see top of Fig. 5(b)], which was consistent with the multi-pulse SM spectrum. Compared with the reported results, the comb-teeth structure in the SC combs spectra generated in the NALM can be easily and effectively controlled by the tunable SM fiber laser in our experiment.

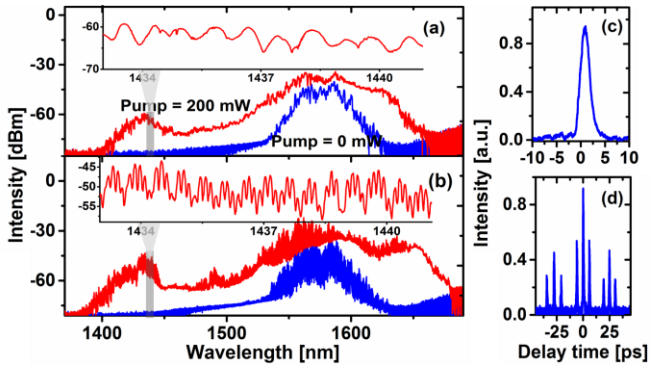

Fig. 5. Output spectra of the SC combs generated by different soliton pulses: (a) single SP, (b) multi-pulse SM; (c) and (d) the corresponding intensity autocorrelation trace of single SP and multi-pulse SM.

To get more insight into the dynamics of dual SC combs generation, we conducted numerical simulation of the signal interaction in both the arms of the NALM. The clockwise (A_1) and counterclockwise (A_2) propagating pulses in NALM were

defined as: $A_1 = A_{in}\sqrt{1/2}$, $A_2 = A_{in} i\sqrt{1/2}$. Clockwise propagating envelope A_1 was first multiplied by an EDF amplifier with positive gain factor g in 30-nm gain bandwidth, and then the signal propagation in the HNLF was simulated using generalized nonlinear Schrödinger equation (GNLSE) [31, 32]:

$$\frac{\partial A_{1,2}(z,t)}{\partial z} = -\frac{\alpha}{2}A_{1,2}(z,t) - \frac{i\beta_2}{2}\frac{\partial^2 A_{1,2}(z,t)}{\partial t^2} + \frac{\beta_3}{6}\frac{\partial^3 A_{1,2}(z,t)}{\partial t^3}$$
$$+ i\gamma\left(1 + i\tau_{shock}\frac{\partial}{\partial t}\right)A_{1,2}(z,t) \times \int_{-\infty}^{+\infty} R(t')\left|A_{1,2}(z,t-t')\right|^2 dt', \quad (1)$$

where α is the loss coefficient, β_2, β_3 represent the second-order, third-order dispersion respectively, γ denotes the nonlinear coefficient. $\tau_{shock} = 1/\omega_0$ where ω_0 is the center frequency, $R(t) = (1 - f_R)\delta(t) + f_R h_R(t)$ is the Raman response function (f_R and h_R are based on the experimental fused silica Raman cross-section) [33].

For the counter-clockwise propagating pulse envelope A_2 the propagation through the HNLF was simulated before multiplication with the amplification gain factor. The transmitted (A_t, output 1) and reflected (A_r, output 2) amplitudes were calculated as follows:

$$A_t = \overline{A_2}\sqrt{\frac{1}{2}} - i\overline{A_1}\sqrt{\frac{1}{2}}, \quad A_r = \overline{A_1}\sqrt{\frac{1}{2}} - i\overline{A_2}\sqrt{\frac{1}{2}}. \quad (2)$$

where $\overline{A_1}$, $\overline{A_2}$ were the counter propagating pulses amplitudes after signals propagation in the NALM. In the NALM, the evolution along the spatial coordinate z of both counter propagating pulses amplitudes $A_{1,2}(z,t)$ were simulated using GNLSE with α = 0.935 dB/km, β_2 = –0.7 ps^2/km, β_3 = –0.022 ps^3/km, γ = 9.4/W/km, L = 0.585 km, $\omega_0 = 1.2075 \times 10^3$ rad/ps.

First set of simulations was carried out with single SP as the initial condition (pulse duration –1.7 ps and peak power –6.8 W) injected into the NALM. Figs. 6(a), (b) depicted the SC spectrum at output 2 and the corresponding temporal pulse profile (blue curves – simulation results and red curves – experimental results). Simulation results also confirmed that the comb-like structure not formed in the spectrum for the case of SP injected into the NALM. Compared with the injected SP, the NALM output signal has a series of separated shorter-duration pulses, which are on their own fundamental solitons formed by the typical nonlinear process for picosecond SC generation [32]. For the second set of simulations, a soliton molecule pair is injected into the NALM, and the pulse parameters are kept the same as that of the experiment. The spectral and temporal characteristics of SC comb are presented in Figs 6(c) and (d), which result from an ensemble of 112 simulations. Experimentally measured spectral modulation depth was lower than the calculated value from the numerical result, but the profiles overlapped well. Finer spectral structure of the generated SC comb is shown in Fig. 6(c), as zoomed-in view of the spectral region range of 1540.9–1548.8 nm. This again confirms that the comb-teeth structure fits well between the experiment and the simulation. The corresponding output temporal pulse is shown in Fig. 6(d). The soliton pulses bound in SM have broken up into several individual shorter pulses, and the number of shorter pulses and intensity fluctuations are consistent between experiments and simulations results. Figure 6(e) shows the level of first-order coherence of the SC signal calculated from the ensemble results. The spectral coherence (blue curve) of the SC generated from SP is almost close to unity in the whole wavelength range of the SC. Coherence values deviating away from unity were contributed by the wider gap between the spikes appeared in the SC spectra around the same wavelength. For the SC comb generated by SM, the spectral coherence (red curve) shows a periodic modulation, which corresponds to the comb-like structure in the SC spectrum.

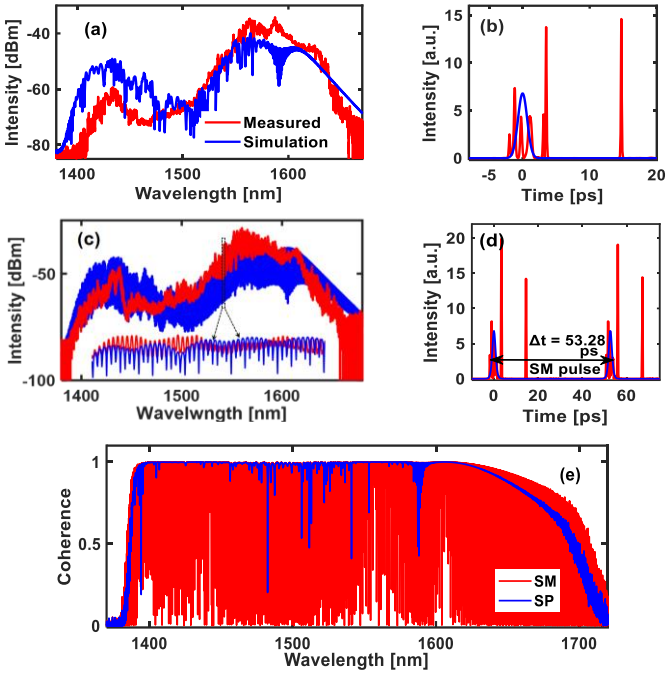

Fig. 6. (a) Simulated and measured SC comb generated by SP, and (b) is the output temporal pulses; (c) simulated and measured SC combs generated by SM, and (d) is the output temporal pulses; (e) first-order coherences of SC comb generated by SP and SM.

4. Conclusions

To conclude, for the very first time, we experimentally demonstrated the possibility of SC comb generation in a cascaded optical setup of tunable soliton molecule mode-locked laser and NALM. Compared with the conventional laser synthesizer with phase correlation and multistage EO modulator schemes, our proposed experimental setup provides a novel method for dual comb-like SC signals generation in HNLF, and this system is compact and economical. Additionally, the SC combs with different comb-teeth structures can be flexibly achieved by controlling the versatile SM generation in PM mode-locked fiber laser that can be potentially utilized in bioluminescent imaging and broadband spectrometers. Maximum obtainable output powers of SC combs from two ports were 21.95 and 3.75 mW. Numerical simulations results matched very well with the experimental results for both cases of injecting SP and SM into the NALM, and the calculated first-order coherence throughout the spectral range of the SC combs is very good.

Funding

This work is financially supported by National Natural Science Foundation of China (61805281); Natural Science Foundation of Guangdong Province, China (2019A1515010732).

References

1. N. Picqué, and T. W. Hänsch, "Frequency comb spectroscopy," *Nat. photon.*, 13(2019), 146.
2. Hu H *et al.*, "Single-source chip-based frequency comb enabling extreme parallel data transmission," *Nat. Photon.*, 12(2018), 469.
3. Cundiff S T, Weiner A M. "Optical arbitrary waveform generation," *Nat. Photon.*, 4(2010), 760.
4. A. Kovach *et al.*, "Emerging material systems for integrated optical Kerr frequency combs," *Adv. Opt. and Photon.*, 12(2020), 135–222.
5. A. Parriaux, K. Hammani, and G. Millot, "Electro-optic frequency combs," *Adv. Opt. and Photon.*, 12(2020), 223.
6. S. Choi *et al.*, "Supercontinuum comb generation using optical pulse synthesizer and highly nonlinear dispersion-shifted fiber," *Jpn. J. Appl. Phys.*, 48(2009), 09LF01.
7. S. Choi *et al.*, "Multi-gigahertz frequency comb-based interferometry using frequency-variable supercontinuum generated by optical pulse synthesizer," *Opt. Express*, 20(2012), 27820.
8. Yoshida M *et al.*, "1.55 μm hydrogen cyanide optical frequency-stabilized and 10 GHz repetition rate stabilized mode-locked fiber laser," *Opt. Express*, 24(2016), 24287.
9. J. Han *et al.*, "10-GHz broadband optical frequency comb generation at 1550/1310 nm," *Opto-Electronic Adv.*, 3(2020), 190033.
10. R. Wu *et al.*, "Supercontinuum-based 10-GHz flat-topped optical frequency comb generation," *Opt. Express*, 21(2013), 6045.
11. V. Torres-Company and A M. Weiner, "Optical frequency comb technology for ultra-broadband radio-frequency photonics," *Laser Photonics Rev.*, 8(2014), 368.
12. B. A. Malomed, "Bound solitons in the nonlinear Schrödinger/ Ginzburg-Landau equation," *Phys. Rev. A*, 44(1991), 6954.
13. D. Y. Tang *et al.*, "Observation of bound states of solitons in a passively mode-locked fiber laser," *Phys. Rev. A*, 64(2001), 033814.
14. N. H. Seong and D. Y. Kim, "Experimental observation of stable bound solitons in a figure-eight fiber laser," *Opt. Lett.*, 27(2002), 1321.
15. A. Kokhanovskiy, E. Kuprikov, S. Kobtsev, "Single- and multi-soliton generation in figure-eight mode-locked fibre laser with two active media," *Opt. Laser Technol*. 131(2020), 106422.
16. L. Gui, X. Xiao, and C. Yang, "Observation of various bound solitons in a carbon-nanotube-based erbium fiber laser," *J. Opt. Soc. Am. B*, 30(2003), 158.
17. B. Fu *et al.*, "Bound states of solitons in a harmonic graphene-mode-locked fiber laser," *Photon. Res.* 7(2019), 116.
18. Y. Cao *et al.*, "Experimental revealing of fiber laser soliton build-up activated by shaking-soliton triplets," *Opt. Laser Technol*. 147(2022), 107677.
19. R. Lü *et al.*, "Soliton and bound-state soliton mode-locked fiber laser based on a MoS_2/fluorine mica Langmuir–Blodgett film saturable absorber," *Photon. Res.* 7(2019), 431.
20. T. Zhu *et al.*, "Observation of controllable tightly and loosely bound solitons with an all-fiber saturable absorber," *Photon. Res.* 7(2019), 61.
21. H. Qin *et al.*, "Observation of soliton molecules in a spatiotemporal mode-locked multimode fiber laser," *Opt. Lett.*, 43(2018), 1982.
22. Y. Wang *et al.*, "Universal mechanism for the binding of temporal cavity solitons," *Optica*, 4(2017), 855.
23. L. Li *et al.*, "Various soliton molecules in fiber systems," *Appl. Opt.*, 10(2019), 2745.
24. R. Zhou *et al.*, "Observation of soliton molecules in a robust all PM mode-locked fiber laser with nonreciprocal phase bias," *IEEE Photon. J*, 13(2021), 1500210.
25. D. Y. Tang, L. M. Zhao, and B. Zhao, "Multipulse bound solitons with fixed pulse separations formed by direct soliton interaction," *Appl. Phys. B*, 80(2005), 239.
26. D. Y. Tang, B. Zhao, and L. M. Zhao, "Soliton interaction in a fiber ring laser," *Phys. Rev. E*, 72(2005), 016616.
27. E. Myslivets *et al.*, "Generation of wideband frequency combs by continuous-wave seeding of multistage mixers with synthesized dispersion," *Opt. Express*, 20(2012), 3331.
28. T. Yang *et al.*, "Comparison analysis of optical frequency comb generation with nonlinear effects in highly nonlinear fibers," *Opt. Express*, 21(2013), 8508.
29. Y. Wang *et al.*, "Soliton distillation of pulses from a fiber laser," *J. Light. Technol.*, 39(2021), 2542.
30. S. M. Kobtsev and S. V. Kukarin, "All fiber Raman supercontinuum generator," *Laser Phys.*, 20(2010), 372.
31. C. Huang, K. Nakkeeran and Q. Li, "Control of long pulse pumped supercontinuum generation using weak trigger signal," *J. Light. Technol.*, 38(2020), 1506.
32. J. M. Dudley, G. Genty, and S. Coen, "Supercontinuum generation in photonic crystal fiber," *Rev. Modern Phys.*, 78(2006), 1135.
33. R. H. Stolen *et al.*, "Raman response function of silica-core fibers," *J. Opt. Soc. Am. B*, 6(1989), 1159.